Model Predictive Pulse Pattern Control

Tobias Geyer, *Senior Member, IEEE,* Nikolaos Oikonomou, *Member, IEEE*,
Georgios Papafotiou, *Member, IEEE,* and Frederick Kieferndorf, *Member, IEEE*

***Abstract*—Industrial applications of medium-voltage drives impose increasingly stringent performance requirements, particularly with regards to harmonic distortions of the phase currents of the controlled electrical machine. An established method to achieve very low current distortions during steady-state operation is to employ offline calculated optimized pulse patterns (OPP). Achieving high dynamic performance, however, proves to be very difficult in a system operated by OPPs.**

In this paper, we propose a method that combines the optimal steady-state performance of OPPs with the very fast dynamics of trajectory tracking control. A constrained optimal control problem with a receding horizon policy, i.e. model predictive control (MPC), is formulated and solved. Results show that the combination of MPC with OPPs satisfies both the strict steady-state as well as the dynamic performance requirements imposed by the most demanding industrial applications. This is achieved without resorting to complicated structures such as observers of the state variable fundamental components of the electrical machine, which are required by state-of-the-art methods. A further advantage of the MPC method is the use of a receding horizon policy to provide feedback and a high degree of robustness.

***Index Terms*—AC drive, optimized pulse pattern, pulse width modulation, trajectory tracking control, model predictive control**

I. Introduction

Medium-voltage ac drives are operated at low switching frequencies to minimize the switching losses of the power semiconductors in the inverter. However, lowering the switching frequency typically increases the harmonic distortions of the stator currents, resulting in high harmonic losses in the electrical machine. One solution is to employ offline calculated pulse patterns in the inverter's modulator that minimize the current harmonics for a given switching frequency.

Traditionally, however, it has only been possible to use such optimized pulse patterns (OPPs) in a modulator driven by a very slow control loop. This leads to a poor dynamic performance and to harmonic excursions of the stator currents when the operating point is changed or when transitions between different pulse patterns occur.

This paper describes a novel control and modulation strategy, based on OPPs, that enables very fast response times during transients, a fast rejection of disturbances, and a nearly optimal ratio of harmonic current distortion per switching frequency at steady-state operation. These OPPs are computed in an offline procedure by calculating the switching angles over a quarter fundamental period for all possible operating points [1], [2]. Typically, the objective is to minimize the harmonic current distortion for a given switching frequency.

T. Geyer is currently with the Department of Electrical and Computer Engineering, The University of Auckland, New Zealand; e-mail: t.geyer@ieee.org
N. Oikonomou, G. Papafotiou and F. Kieferndorf are with ABB Corporate Research, Baden-Dättwil, Switzerland; e-mails: nikolaos.oikonomou@ch.abb.com, georgios.papafotiou@ch.abb.com and frederick.kieferndorf@ch.abb.com

When field oriented control (FOC) is used to command a pulse width modulator that employs OPPs, the performance of the overall control scheme is very limited, even in quasi steady-state operation. Excursions of the harmonic currents occur that may lead to overcurrent conditions [3]. Thus, the application of field oriented current control with OPPs is typically limited to grid-connected setups, where the operating range is relatively small. When the goal is to use this method in applications with widely varying operating points, as is the case for electrical machine control, the (inner) current control loop is tuned to be very slow, such that its operation does not interfere with the optimal volt-second balance of the OPPs. However, such a tuning significantly decreases the dynamic performance of the drive.

As an improvement to FOC with OPPs, *current trajectory* tracking was proposed in [4]. This method derives the optimal steady-state stator current trajectory from the pulse pattern in use. The actual stator current space vector is forced to follow this target trajectory. A disadvantage is that the stator current trajectory depends on the parameters of the electrical machine, specifically on the total leakage inductance [5]. Changing load conditions have also been found to influence the stator current trajectory.

A further improvement can be made by tracking the *stator flux trajectory* [6], which is insensitive to parameter variations and is thus better suited for tracking control. By controlling the stator flux space vector to coincide with its optimal trajectory, harmonic excursions are avoided that might appear when the operating point changes. The method is however complex, as it requires an observer to identify the instantaneous fundamental components of the stator current and flux linkage vectors [7]. These signals are not readily available when using OPPs [5], since the harmonic current is not zero at the sampling instants. As a result, the fundamental machine quantities cannot be directly sampled when using OPPs. This makes the design of the closed-loop controller difficult, because these signals are required to achieve flux and torque control. For this reason, existing control schemes, such as [4], [8], employ an observer to derive the instantaneous fundamental current and flux linkage values separately from the respective harmonic quantities.

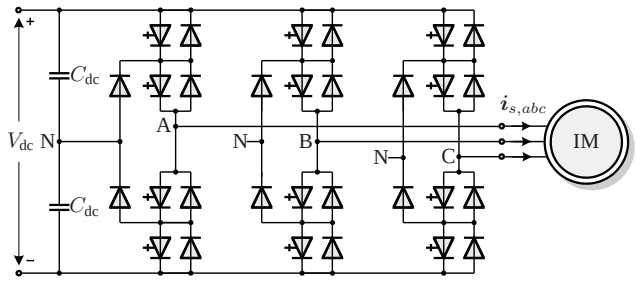

Fig. 1: Three-level neutral point clamped VSI driving an induction machine

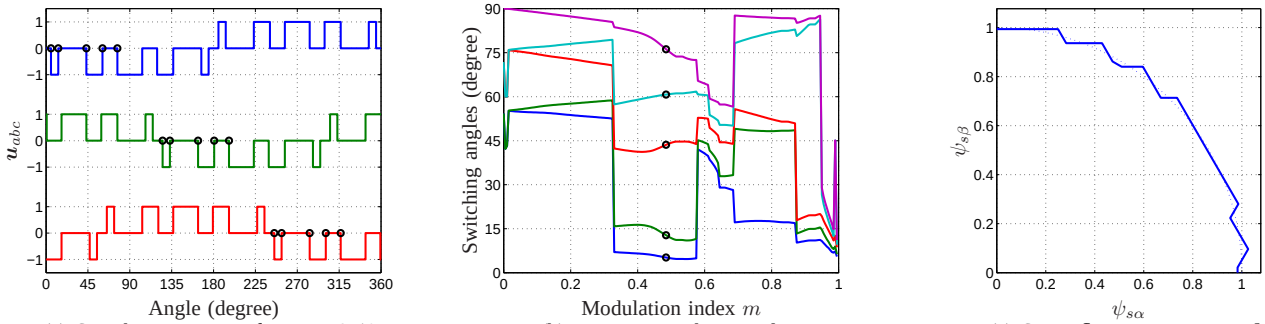

(a) Switching sequence for $m = 0.48$ (b) Primary switching angles (c) Stator flux trajectory in $\alpha\beta$

Fig. 2: Optimal pulse pattern with $d = 5$ primary switching angles for a three-level inverter. The three-phase switching sequence and the stator flux trajectory correspond to the modulation index $m = 0.48$. The primary switching angles are indicated by (black) circles

For reliability, simplicity of implementation and dynamic performance reasons, the following three aims are targeted: First, it is desirable to perform trajectory tracking control of the stator flux vector without the need of a complex observer to track the fundamental component of the stator flux or current in real-time. This is one of the advantages of the concept introduced in this paper. Second, the controller should have reduced sensitivity to parameter variations and measurement noise. Third, fast dynamic control is to be achieved while performing the minimum possible modification of the offline calculated pulse pattern sequences. These three objectives are achieved by the controller proposed in this paper. The stator flux trajectory controller is generalized, by formulating it as a constrained optimal control problem with a receding horizon policy, i.e. as model predictive control (MPC) [9]–[11].

Specifically, a prediction horizon of finite length in time is used and the switching instants of the pulse pattern are shifted such that a stator flux error is corrected within this horizon. From the end of the horizon onwards, steady-state operation is assumed. The underlying optimization problem is solved in real-time, yielding a sequence of optimal control actions over the horizon. Only the first control action of this sequence is applied to the drive system, in accordance with the so-called receding horizon policy. At the next sampling instant, the control sequence is recomputed over a shifted horizon, thus providing feedback and robustness to model inaccuracies. A long horizon also renders the controller less susceptible to measurement noise. The receding horizon policy is illustrated in Fig. 3.

In this case, the underlying optimization problem constitutes a quadratic program (QP), which can be solved efficiently in real time by approximation. It is also shown that a further simplification yields the deadbeat (DB) trajectory controller proposed in [6], which thus constitutes a special case of the (more general) MPC controller introduced in this paper.

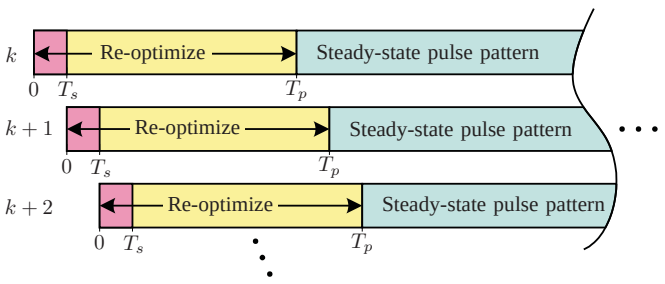

Fig. 3: Illustration of the receding horizon policy. The pulse pattern is re-optimized over the prediction horizon T_p, but only the pattern over the sampling interval T_s is applied to the drive

II. Drive System Case Study

Throughout this paper, we will use normalized quantities. All variables $\boldsymbol{\xi}_{abc} = [\xi_a \ \xi_b \ \xi_c]^T$ in the three-phase system (abc) are transformed to $\boldsymbol{\xi}_{\alpha\beta} = [\xi_\alpha \ \xi_\beta]^T$ in the stationary orthogonal $\alpha\beta$ coordinates through $\boldsymbol{\xi}_{\alpha\beta} = \boldsymbol{P}\,\boldsymbol{\xi}_{abc}$ with

$$\boldsymbol{P} = \frac{2}{3}\begin{bmatrix} 1 & -\frac{1}{2} & -\frac{1}{2} \\ 0 & \frac{\sqrt{3}}{2} & -\frac{\sqrt{3}}{2} \end{bmatrix}, \quad \boldsymbol{P}^{-1} = \begin{bmatrix} 1 & 0 \\ -\frac{1}{2} & \frac{\sqrt{3}}{2} \\ -\frac{1}{2} & -\frac{\sqrt{3}}{2} \end{bmatrix}. \quad (1)$$

$\boldsymbol{P}^{-1}$ denotes the pseudo-inverse of $\boldsymbol{P}$.

As an illustrative example of a medium-voltage variable speed drive system consider a three-level neutral point clamped (NPC) voltage source inverter (VSI) driving an induction machine (IM), as depicted in Fig. 1. The total dc-link voltage V_{dc} over the two dc-link capacitors C_{dc} is assumed to be constant.

Let the integer variables u_a, u_b, $u_c \in \{-1, 0, 1\}$ denote the switch positions in each phase leg, where the values $-1, 0, 1$ correspond to the phase voltages $-\frac{V_{\text{dc}}}{2}, 0, \frac{V_{\text{dc}}}{2}$, respectively. The actual voltage applied to the machine terminals is given by $\boldsymbol{v}_{\alpha\beta} = 0.5 V_{\text{dc}}\,\boldsymbol{P}\,\boldsymbol{u}_{abc}$ with $\boldsymbol{u} = \boldsymbol{u}_{abc} = [u_a \ u_b \ u_c]^T$.

III. Optimized Pulse Patterns

A. Offline Computation

When computing OPPs, a single-phase pulse pattern is typically considered and quarter-wave symmetry is imposed. The pulse patterns of the phases a, b and c are obtained by shifting the single-phase pattern by 0, 120 and 240 degrees, respectively. As a result, the three-phase pulse pattern over 360 degrees is fully characterized by the single-phase pattern over 90 degrees, see Fig. 2(a).

To compute the single-phase OPP over 90 degrees, the number of primary switching angles (the pulse number) d needs to be selected. An objective function is chosen for the optimization—a common selection is the weighted sum of the squared differential-mode voltage harmonics, which is effectively equivalent to the total harmonic distortion (THD) of the current. For every value of the modulation index,

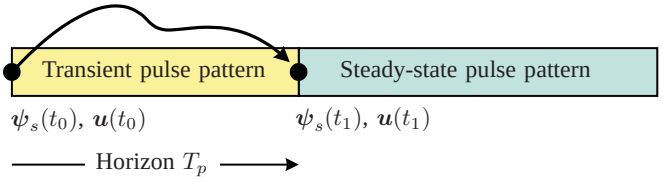

Fig. 4: Boundary control problem formulated over the horizon T_p. The transient pulse pattern drives the stator flux vector $\boldsymbol{\psi}_s$ from time t_0 to t_1 and links the switch positions $\boldsymbol{u}$

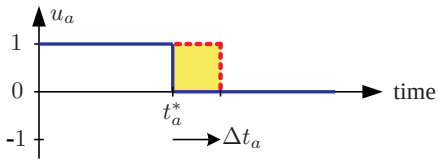

Fig. 5: Delaying the negative switching transition $\Delta u_a = -1$ in phase a by Δt_a, with regards to the nominal switching time t_a^*, increases the stator flux component in this phase by $0.5V_{\text{dc}}(-\Delta u_a)\Delta t_a$

this objective function is minimized by optimizing over the switching angles. This leads to a set of switching angles as a function of the modulation index, characterizing the OPP as shown in Fig. 2(b). For more details on the computation of OPPs for multi-level inverters, see for example [12].

B. Stator Flux Trajectory

Consider an electrical machine connected to the inverter terminals and neglect the machine's stator resistance. The steady-state stator flux trajectory in stationary coordinates, which corresponds to the OPP in use, is obtained by integrating the switched voltage sequence $\boldsymbol{v}_{\alpha\beta}$ over time. Specifically, the stator flux vector $\boldsymbol{\psi}_s = [\psi_{s\alpha}\ \psi_{s\beta}]^T$ at time t is given by

$$\boldsymbol{\psi}_s(t) = \boldsymbol{\psi}_s(0) + \frac{V_{\text{dc}}}{2}\int_0^t \boldsymbol{P}\,\boldsymbol{u}_{abc}(\tau)d\tau\,. \qquad (2)$$

An example steady-state stator flux trajectory in stationary coordinates is shown in Fig. 2(c) over 90 degrees. The average amplitude of the stator flux trajectory is one, yet it is obvious from Fig. 2(c) that the instantaneous amplitude of the stator flux oscillates. The instantaneous angle of the stator flux vector also oscillates around its nominal value. This ripple is the result of variations in the instantaneous angular speed of the stator flux vector, which necessarily arise when applying voltage vectors of different and discrete magnitudes. The ripples on the magnitude and angle of the stator flux vector dictate the discrete frequency spectrum of the current harmonics.

IV. Model Predictive Pulse Pattern Control

Closed-loop control of an electrical machine based on OPPs can be achieved by controlling the stator flux vector along its reference trajectory. The magnitude of the stator flux trajectory determines the magnetization current of the machine, while the angle between the stator and the rotor flux vectors determines the electromagnetic torque.

The flux error vector is the vector difference between the reference flux trajectory and the actual trajectory of the stator flux of the machine. Even at steady-state, this flux error vector is generally non-zero due to non-idealities of the real-world drive system. These non-idealities include fluctuations in the dc-link voltage, the presence of the stator resistance, neglected in (2), and non-idealities of the power inverter, such as dead-time effects. During transient operation, the flux error vector is an accurate mapping of the change in the operating point.

A. Stator Flux Control Problem

The stator flux control problem can be interpreted as a boundary control problem, as illustrated in Fig. 4. Starting at time t_0 with the switch position $\boldsymbol{u}(t_0)$ and the stator flux $\boldsymbol{\psi}_s(t_0)$, a *transient* pulse pattern over the time-interval T_p is to be derived. This pulse pattern drives the stator flux vector to the terminal stator flux $\boldsymbol{\psi}_s(t_1)$ and leads to the terminal switch position $\boldsymbol{u}(t_1)$. In this boundary control problem, $\boldsymbol{u}(t_0)$ and $\boldsymbol{\psi}_s(t_0)$ are the initial conditions, while $\boldsymbol{u}(t_1)$ and $\boldsymbol{\psi}_s(t_1)$ are accordingly the terminal conditions.

The requirements for the transient pulse pattern include the following: First, the transient pattern is required to be optimal in the sense that it minimizes the current and/or torque THD. It is also conceivable that the pulse pattern minimizes the switching losses of the power converter switches, e.g. by penalizing commutation angles that occur at high currents. Next, excessive excursions of the stator flux and thus of the stator currents are to be avoided to prevent over-current conditions. Finally, the torque and the stator flux magnitude are to be controlled around their references—at steady-state operating conditions as well as during transients.

B. Principle of Model Predictive Pulse Pattern Control

The above stated control problem can be formulated as a constrained optimal control problem with a so-called receding horizon policy or, equivalently, as a model predictive control (MPC) problem [11]. The key idea is to associate the prediction horizon with the time interval $T_p = t_1 - t_0$, and to drive the stator flux vector over this horizon to its desired position, thus correcting the stator flux error. From the end of the horizon onwards, steady-state operation is assumed. In particular, the controller *assumes* that from t_1 onwards the original, i.e. the *steady-state* pulse pattern, will be applied. It is crucial to note, however, that due to the receding horizon policy highlighted in the introduction and in Fig. 3, the steady-state OPP will *never* be applied. Instead, at every time-step, the first part of the modified OPP, i.e. the pattern over the sampling interval T_s, will be applied to the drive system.

Under steady-state operating conditions, the stator flux error is small, typically amounting to one to two percent of the nominal flux magnitude. Therefore, only small corrections of the switching instants are required to remove the flux error over the horizon. As a result, the steady-state OPP can be used as a baseline pattern while deriving the transient pulse pattern. This greatly simplifies the control problem at hand, since re-optimizing the OPP around its optimum is significantly less computationally demanding than computing an entirely new transient pulse pattern from scratch.

The control objective is then to regulate the stator flux vector along its given reference trajectory in stationary coordinates, by modifying the switching instants of the OPP within the horizon as little as possible. As an example, consider phase a. According to (2), shifting the switching transition by the scalar time Δt_a changes the phase a stator flux by

$$\Delta\psi_{sa}(\Delta t_a) = -\frac{V_{\text{dc}}}{2}\Delta u_a \Delta t_a\,, \qquad (3)$$

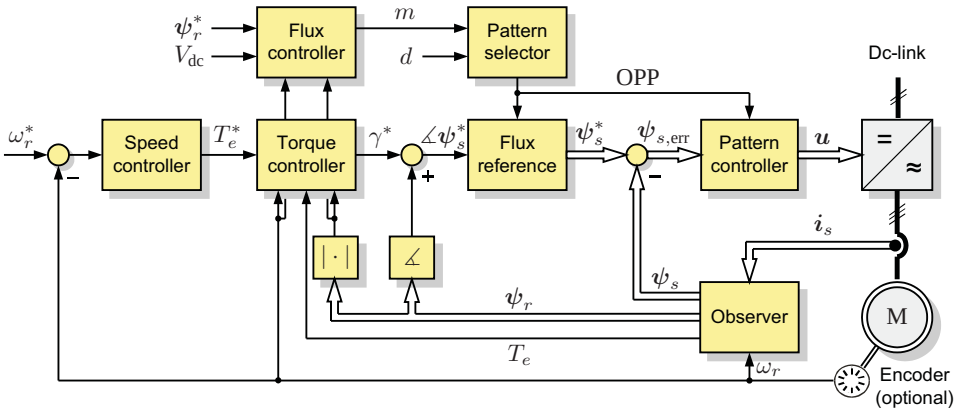

Fig. 6: Block diagram of the model predictive pulse pattern control (MP^{3}C) scheme

where, $\Delta u_a = u_a(t_a^*) - u_a(t_a^* - \mathrm{d}t)$ denotes the switching transition in phase a, with $\Delta u_a \in \{-1, 1\}$. The nominal switching time is given by t_a^* and $\mathrm{d}t$ is an infinitesimally small time step. All variables are given in per unit.

An example is shown in Fig. 5. Delaying the negative switching transition $\Delta u_a = -1$ by Δt_a increases the volt-seconds and thus the stator flux in this phase. Advancing the switching event has the opposite effect, i.e. it decreases the flux amplitude in the direction of phase a. The same holds for phases b and c.

Compensation of the flux error vector in real time by modifying the switching instants of the OPP, results in fast closed-loop control. We refer to this control concept as model predictive pulse pattern control (MP^{3}C).

C. Optimality

It is important to point out that, as indicated above, optimality, i.e. minimal current THD, is achieved when the reference stator flux trajectory is accurately tracked. Optimality is thus defined in terms of the reference flux trajectory rather than in terms of the steady-state voltage waveform. These two terms coincide only at steady-state under ideal conditions. Optimality can also be achieved for quasi steady-state conditions, by ensuring that the reference flux trajectory is closely tracked.

During large transients, when major torque steps are applied or when switching between different pulse patterns, the stator flux error tends to be large and significant corrections of the switching instants are mandatory. As a result, the transient pulse pattern obtained by re-optimizing around the existing OPP might be suboptimal. However, the notion of harmonic distortion, which is based on the frequency analysis, is not meaningful during such transients. Therefore, rather than focusing on a minimal current THD, during transients the controller aims at achieving a very fast dynamic response by rapidly tracking the new stator flux reference trajectory.

D. Proposed MP^{3}C Algorithm

The proposed MP^{3}C algorithm is shown in the block diagram in Fig. 6. It operates in the discrete time domain and is activated at equally spaced time-instants kT_s, with $k \in \mathbb{N}$ being the discrete time-step and T_s denoting the sampling interval. The control problem is formulated and solved in stationary orthogonal coordinates. The angular electrical stator and rotor frequencies of the machine are ω_s and ω_r, respectively. The algorithm comprises the following six steps, which are executed at the time-instant kT_s.

Step 1. Estimate the stator and rotor flux vectors in the stationary reference frame. This yields $\boldsymbol{\psi}_s = [\psi_{s\alpha}\ \psi_{s\beta}]^T$ and $\boldsymbol{\psi}_r = [\psi_{r\alpha}\ \psi_{r\beta}]^T$. Let $\angle\boldsymbol{\psi}$ denote the angular position of a flux vector and $|\boldsymbol{\psi}|$ its magnitude.

Compensate for the delay introduced by the controller computation time by rotating the estimated stator and rotor flux vectors by $\omega_s T_s$ forward in time, i.e. $\angle\boldsymbol{\psi}_s = \angle\boldsymbol{\psi}_s + \omega_s T_s$ and accordingly for the rotor flux.

Step 2. Compute the reference of the stator flux vector $\boldsymbol{\psi}_s^*$. Recall that the electromagnetic torque T_e produced by the machine can be written as $T_e = k_r |\boldsymbol{\psi}_s|\,|\boldsymbol{\psi}_r| \sin(\gamma)$, where k_r is the rotor coupling factor, and γ is the angle between the stator and the rotor flux vectors. When the machine is fully magnetized, the magnitude of the reference flux vector is equal to 1 pu. Then, for a given value of the rotor flux magnitude and a given torque reference, the desired angle between the stator and rotor flux vectors is

$$\gamma^* = \sin^{-1}\left(\frac{T_e^*}{k_r |\boldsymbol{\psi}_r|}\right). \tag{4}$$

The reference flux vector is then obtained by integrating the chosen nominal three-phase pulse pattern; the reference angle $\angle\boldsymbol{\psi}_r + \gamma^*$ constitutes the upper limit of the integral. The resulting instantaneous reference flux vector has, in general, a magnitude and angle that slightly differ from their respective values on the unitary circle, Fig. 7. The vector diagram in this figure provides a graphical summary of the derivation of the reference flux vector.

Step 3. Compute the stator flux error, which is the difference between the reference and the estimated stator flux vector

$$\boldsymbol{\psi}_{s,\mathrm{err}} = \boldsymbol{\psi}_s^* - \boldsymbol{\psi}_s\,. \tag{5}$$

It is evident that this error can be directly calculated—neither the fundamental component nor the harmonic content of the stator flux need to be estimated for this.

Step 4. This step comprises the actual pulse pattern controller. The MP^{3}C control problem can be formulated as an optimization problem with a quadratic objective function and linear constraints, a so called quadratic program (QP). The objective function penalizes both the uncorrected flux error (the controlled variable) and the changes of the switching instants

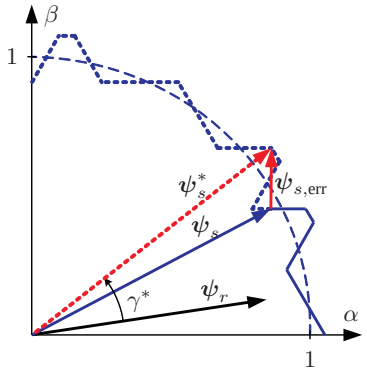

Fig. 7: Actual stator flux vector $\boldsymbol{\psi}_s$, rotor flux vector $\boldsymbol{\psi}_r$, reference flux vector $\boldsymbol{\psi}_s^*$ and stator flux error $\boldsymbol{\psi}_{s,\text{err}}$ in the stationary coordinates

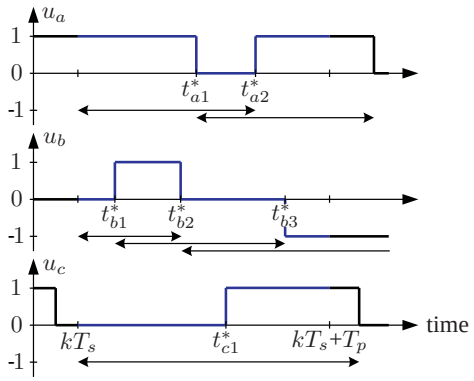

Fig. 8: Model predictive pulse pattern control (MP^{3}C) problem for a three-phase three-level pulse pattern. Six switching transitions fall within the horizon T_p, which is of fixed length. The lower and upper bounds for the nominal switching instants are depicted by arrows

(the manipulated variable), using the weight q. Constraints on the switching instants ensure that the correct sequence of switching transitions is kept and that transitions are not moved into the past. Specifically, the QP is formulated as

$$\min_{\Delta \boldsymbol{t}} \Big(\underbrace{|\boldsymbol{\psi}_{s,\text{err}} - \boldsymbol{\psi}_{s,\text{corr}}(\Delta \boldsymbol{t})|^2 + q \Delta \boldsymbol{t}^T \Delta \boldsymbol{t}}_{J(\Delta \boldsymbol{t})} \Big) \tag{6a}$$

$$\text{s.t. } kT_s \le t_{a1} \le t_{a2} \le \ldots \le kT_s + T_p \tag{6b}$$

$$kT_s \le t_{b1} \le t_{b2} \le \ldots \le kT_s + T_p \tag{6c}$$

$$kT_s \le t_{c1} \le t_{c2} \le \ldots \le kT_s + T_p \,. \tag{6d}$$

Again, $\boldsymbol{\psi}_{s,\text{err}}$ is the stator flux error in stationary coordinates ($\alpha\beta$), $\boldsymbol{\psi}_{s,\text{corr}}(\Delta \boldsymbol{t})$ is the correction of the stator flux, and $\Delta \boldsymbol{t} = [\Delta t_{a1}\ \Delta t_{a2} \ldots \Delta t_{b1} \ldots \Delta t_{c1} \ldots]^T$ denotes the vector of switching instant corrections. For phase a, for example, the correction of the i-th transition time is given by $\Delta t_{ai} = t_{ai} - t_{ai}^*$, where t_{ai}^* denotes the nominal switching instant of the i-th transition Δu_{ai}. Again, the latter is defined as $\Delta u_{ai} = u_a(t_{ai}^*) - u_a(t_{ai}^* - \mathrm{d}t)$ with $\mathrm{d}t$ being an infinitesimally small time step.

The stator flux correction is obtained by rewriting (3)

$$\boldsymbol{\psi}_{s,\text{corr}}(\Delta \boldsymbol{t}) = -\frac{V_\text{dc}}{2} \boldsymbol{P} \begin{bmatrix} \sum_i \Delta u_{ai} \Delta t_{ai} \\ \sum_i \Delta u_{bi} \Delta t_{bi} \\ \sum_i \Delta u_{ci} \Delta t_{ci} \end{bmatrix} . \tag{7}$$

The switching instants cannot be modified arbitrarily—they are constrained by the current time-instant kT_s as well as by the neighboring switching transitions in the same phase. Fig. 8 provides an example to illustrate this. The first switching transition in phase b, for example, is constrained to lie between kT_s and the nominal switching instant of the second transition in phase b. The second switching transition in phase b can only be delayed up to the nominal switching instant of the third transition in the same phase. Note that the transitions in a given phase are modified independently from those in the other phases.

Step 5. Remove switching transitions from the QP that will occur within the sampling interval. This can be accomplished by updating a pointer to the look-up table that stores the switching angles of the OPP and the respective three-phase potential values.

Step 6. Derive the switching commands over the sampling interval, i.e. the switching instants and the associated switch positions. The switching commands are sent to the gate units of the semiconductor switches in the inverter.

To reiterate, even though a sequence of switch positions is planned over a long prediction horizon, only the switching sequence over the sampling interval is executed. The predictions are recomputed at the next sampling interval using new measurements; a shifted—and if necessary revised—sequence of switch positions is derived. This is referred to as the receding horizon policy, see Fig. 3, which provides feedback and makes MP^{3}C robust to the flux estimation errors and non-idealities mentioned earlier. Longer horizons reduce the controller sensitivity to flux estimation errors. As a result, the steady-state current distortions tend to be lower, when compared with an overly aggressive controller, i.e. a controller that operates with a very short prediction horizon and does not penalize the corrective action ($q = 0$).

E. Outer Control Loops

The inner MP^{3}C control loop described above is augmented by two outer control loops, as shown in Fig. 6. The first loop regulates the torque by adjusting the reference angle between the stator and the rotor flux vectors. The second loop regulates the stator flux magnitude by adjusting the modulation index. The slow stator flux controller uses information from the inner loop of MP^{3}C to adjust the modulation index—specifically, the volt-second correction or the effective modulation index.

V. Computational Aspects

A. Active Set Method to Solve the QP

The QP formulated in Step 4 can be solved efficiently by adopting the so called active set method for quadratic programming. This is a standard approach to solve QPs of small to medium scale. The active set method is described in detail in [13, Sect. 16.4].

We start by computing the unconstrained solution, i.e. we minimize (6a), while neglecting the timing constraints (6b)–(6d). We also recall that the step size of all switching transitions is ± 1, i.e. $|\Delta u_{ai}| = 1$, and accordingly for phases b and c. It is obvious that the resulting modifications of the switching instants are the same per phase. We can thus define $\delta_a = \frac{1}{3} \frac{V_\text{dc}}{2} \Delta t_{ai}$ for phase a, with δ_a denoting the scaled volt-second modification for the phase a transitions. Further, let n_a denote the number of switching transitions in phase a that

occur within the horizon. The variables for phases b and c are defined accordingly.

The per-phase variables defined above can be aggregated to the three-phase vectors $\boldsymbol{\delta} = [\delta_a\ \delta_b\ \delta_c]^T$ and $\boldsymbol{n} = [n_a\ n_b\ n_c]^T$. As an example for the latter, refer to Fig. 8, which corresponds to $\boldsymbol{n} = [2\ 3\ 1]^T$.

Introducing the constant $\varrho = \frac{1}{2}q/(\frac{1}{3}\frac{V_{\text{dc}}}{2})^2$, we can rewrite J in (6a) as

$$J(\boldsymbol{\delta}) = |\boldsymbol{\psi}_{s,\text{err}} - \boldsymbol{\psi}_{s,\text{corr}}(\boldsymbol{\delta})|^2 + 2\varrho\big(n_a\delta_a^2 + n_b\delta_b^2 + n_c\delta_c^2\big) \quad (8)$$

and (7) as $\boldsymbol{\psi}_{s,\text{corr}}(\boldsymbol{\delta}) = -3\boldsymbol{P}\boldsymbol{n}^T\boldsymbol{\delta}$. Setting $\nabla J(\boldsymbol{\delta})$ to zero yields the unconstrained minimum

$$\boldsymbol{\delta} = -\boldsymbol{M}^{-1}\boldsymbol{P}^{-1}\boldsymbol{\psi}_{s,\text{err}} \quad (9)$$

with

$$\boldsymbol{M} = \begin{bmatrix} 2n_a + \varrho & -n_b & -n_c \\ -n_a & 2n_b + \varrho & -n_c \\ -n_a & -n_b & 2n_c + \varrho \end{bmatrix}. \quad (10)$$

The expression $\boldsymbol{M}^{-1}\boldsymbol{P}^{-1}$ can be derived algebraically and does not need to be computed in real time.

The tailored active set method to solve the QP (6) involves several iterations of the following three steps.

Step 1. Compute the number of switching transitions $\boldsymbol{n}$ for each phase that fall within the horizon.

Step 2. Neglect the timing constraints and compute the unconstrained volt-second corrections $\boldsymbol{\delta}$ per phase. Convert these into unconstrained switching instants, taking the sign of the switching transition into account. For the i-th transition in phase a, this implies $t_{ai} = t_{ai}^* + 3\frac{2}{V_{\text{dc}}}\frac{\delta_a}{\Delta u_{ai}}$. Phases b and c are defined accordingly.

Step 3. Impose the timing constraints (6b)–(6d) by determining the switching instants that violate one or more of the constraints (the so-called active constraints). For the active constraints, perform the following operations: limit the unconstrained switching instants by imposing the constraints. This yields the final solution for these switching instants. Remove these switching instants and their associated switching transitions from the optimization problem and reduce $\boldsymbol{n}$ accordingly. Finally, compute the flux correction that results from these modified switching instants and update the remaining (as yet uncorrected) flux error accordingly.

Iterate over Steps 2 and 3 again until the solution remains unchanged. In general, two iterations suffice.

This procedure is computationally simple. Most importantly, the computational complexity is effectively independent of the number of considered switching transitions and thus of the length of the horizon. Specifically, the dimension of the matrix $\boldsymbol{M}^{-1}\boldsymbol{P}^{-1}$ is always 3x2. Since the offline computed OPP always has switching transitions of step-size one, the above outlined active set method yields the same result as the QP formulation (6). Small differences would occur, if some transitions had step-sizes greater than one.

For the rest of the paper we will refer to the method outlined in the present section as *approximate QP* solution. The method of Step 4 of Sect. IV-D will simply be referred to as *QP*.

B. MP^{3}C based on Deadbeat Control

Another alternative is to set the weight q in (6a) to zero. As a result, the degree by which the switching instants are modified is not penalized. The horizon is kept as short as possible. Specifically, the horizon is redefined as the minimum time interval starting at the current time instant such that at least two phases exhibit switching transitions. This leads to a pulse pattern controller with DB characteristic. The control algorithm is computationally and conceptually very simple, as summarized in the following.

Step 1. Determine the two phases that have the next scheduled switching transitions. We refer to those as the *active* phases, which are always pairs, i.e. ab, bc or ac. This also yields the length of the horizon T_p, which is of variable length for the DB controller. Determine all switching transitions within the horizon. In Fig. 8, for example, phases a and b have the next switching transitions and are thus the active phases. Their nominal switching instants are t_{b1}^*, t_{b2}^* and t_{a1}^*. The horizon thus spans the time interval from kT_s to t_{a1}^*.

Step 2. Translate the flux error from $\alpha\beta$ to abc, by mapping it into the two active phases. The flux error of the third phase is zero. For the example above, with the active phases a and b, the mapping is given by $\boldsymbol{\psi}_{s,abc,\text{err}} = \boldsymbol{P}_{ab}^{-1}\boldsymbol{\psi}_{s,\text{err}}$ with

$$\boldsymbol{P}_{ab}^{-1} = \begin{bmatrix} \frac{3}{2} & \frac{\sqrt{3}}{2} \\ 0 & \sqrt{3} \\ 0 & 0 \end{bmatrix}. \quad (11)$$

Step 3. Compute the required modification of the switching instants in abc, given by $\Delta\boldsymbol{t}_{\text{req}} = \boldsymbol{\psi}_{s,abc,\text{err}}/(V_{\text{dc}}/2)$.

Step 4. Go through all switching transitions of the first active phase x, with $x \in \{a, b, c\}$. For the i-th switching transition in this phase with the nominal switching instant t_{xi}^* and the switching transition Δu_{xi}, perform the following operations:

- Compute in a DB fashion the desired modification $\Delta t_{xi} = \Delta t_{x,\text{req}}/(-\Delta u_{xi})$.
- Modify the switching instant to $t_{xi} = t_{xi}^* + \Delta t_{xi}$.
- Constrain t_{xi} by imposing the respective constraints on the switching instant.
- Update the phase x component of the required switching instant modification, by replacing $\Delta t_{x,\text{req}}$ with $\Delta t_{x,\text{req}} - (t_{xi} - t_{xi}^*)(-\Delta u_{xi})$.

Repeat the above procedure for the second active phase.

Note that, only in cases in which the constraints are not active, $t_{xi} - t_{xi}^*$ equals the desired modification Δt_{xi}. Since the DB controller aims at removing the stator flux error as quickly as possible and since corrections in the switching instants are not penalized, the DB controller tends to be very fast and aggressive. Yet, there is no guarantee that the flux error is fully removed within the horizon, since the constraints on the switching instants have to be respected.

Induction motor	Voltage	3300 V	r_s	0.0108 pu
	Current	356 A	r_r	0.0091 pu
	Real power	1.587 MW	x_{ls}	0.1493 pu
	Apparent power	2.035 MVA	x_{lr}	0.1104 pu
	Frequency	50 Hz	x_m	2.3489 pu
	Rotational speed	596 rpm		
Inverter			V_{dc}	1.930 pu
			x_c	11.769 pu

TABLE I: Rated values (left) and parameters (right) of the drive

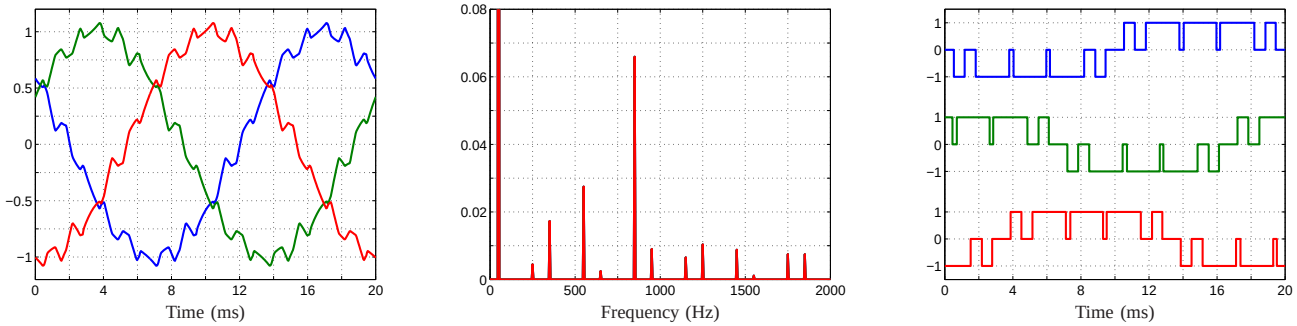

(a) Stator currents $\boldsymbol{i}_s$ (b) Stator current spectrum (c) Switch positions $\boldsymbol{u}$

Fig. 9: Space vector modulation (SVM) at nominal speed and full torque with the carrier frequency $f_c = 450\,\text{Hz}$. The modulation index is $m = 0.82$. The stator currents and the switch positions are shown versus the time-axis in ms, while the stator current spectrum is depicted versus the frequency axis in Hz. All quantities are given in pu

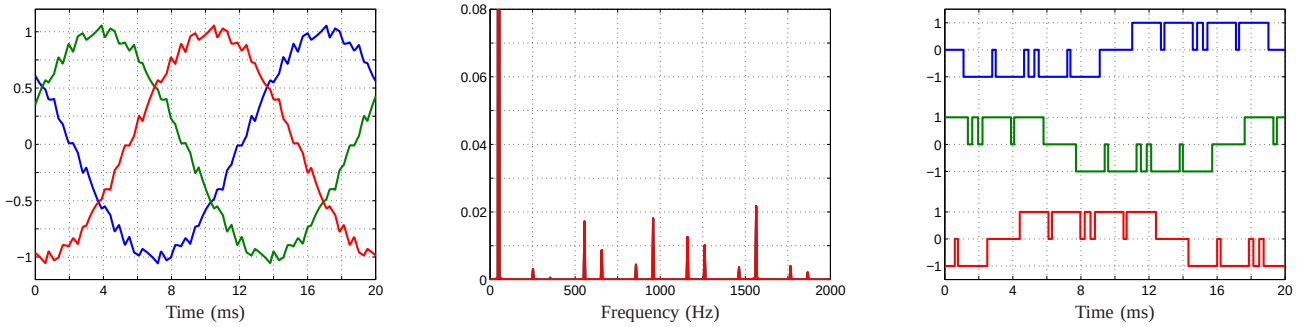

(a) Stator currents $\boldsymbol{i}_s$ (b) Stator current spectrum (c) Switch positions $\boldsymbol{u}$

Fig. 10: Model predictive pulse pattern control (MP^{3}C) with the pulse number $d = 5$. The operating point, the switching frequency, the plots and their scaling are the same as in Fig. 9 to facilitate a direct comparison

VI. Performance Evaluation

As a case study, consider a three-level NPC voltage source inverter driving an induction machine with a constant mechanical load, as shown in Fig. 1. A 3.3 kV and 50 Hz squirrel-cage induction machine rated at 2 MVA with a total leakage inductance of 0.25 pu is used as an example of a typical medium-voltage induction machine. The dc-link voltage is $V_{\text{dc}} = 5.2\,\text{kV}$ and the modulation index (as defined in [5]) is $m = 0.82$ for all cases. The detailed parameters of the machine and the inverter are summarized in Table I. The per unit system is established using the base quantities $V_B = \sqrt{2/3}V_{\text{rat}} = 2694\,\text{V}$, $I_B = \sqrt{2}I_{\text{rat}} = 503.5\,\text{A}$ and $f_B = f_{\text{rat}} = 50\,\text{Hz}$.

A. Steady-State Operating Conditions

At nominal speed and rated torque, closed-loop simulations were run to evaluate the performance of MP^{3}C under steady-state operating conditions. The key performance criteria are the harmonic distortions of the current and torque for a given switching frequency. The simulated MP^{3}C is based on the DB controller and OPPs with various pulse numbers calculated offline according to Sect. III-A. MP^{3}C is compared with two commonly used modulation methods—carrier-based pulse width modulation (PWM) and space vector modulation (SVM). Specifically, a three-level regular sampled PWM is implemented with two in phase triangular carriers, so-called phase disposition (PD). It is generally accepted that for multi-level inverters, carrier-based PWM with PD results in the lowest harmonic distortion. In accordance with common practise, the reference signals are generated by adding a one sixth third harmonic to the modulating reference signals to boost the differential-mode voltage. The SVM is obtained by adopting the approach proposed in [14]: A common mode voltage, which is of the min/max type plus a modulus operation, is added to the reference voltage.

Control scheme	Control setting	f_{sw} [Hz]	$I_{s,\text{THD}}$ [%]	$T_{e,\text{THD}}$ [%]	$I_{s,\text{THD}}$ [%]	$T_{e,\text{THD}}$ [%]
PWM	$f_c = 250\,\text{Hz}$	150	16.1	11.0	100	100
SVM	$f_c = 250\,\text{Hz}$	150	15.5	9.83	96.8	89.6
MP^{3}C	$d = 3$	150	7.36	6.62	45.9	60.3
PWM	$f_c = 450\,\text{Hz}$	250	7.94	5.79	100	100
SVM	$f_c = 450\,\text{Hz}$	250	7.71	5.35	97.1	92.4
MP^{3}C	$d = 5$	250	4.13	3.41	52.0	58.9
PWM	$f_c = 750\,\text{Hz}$	400	4.68	3.41	100	100
SVM	$f_c = 750\,\text{Hz}$	400	4.52	3.06	96.6	89.7
MP^{3}C	$d = 8$	400	3.63	2.88	77.6	84.5

TABLE II: Comparison of MP^{3}C with PWM and SVM in terms of the switching frequency f_{sw}, the current THD $I_{s,\text{THD}}$ and the torque THD $T_{e,\text{THD}}$. The center section shows absolute values, while the values in the right section are relative, using PWM as a baseline. The pulse number is given by d and the carrier frequency by f_c. In all cases the modulation index is $m = 0.82$

At steady-state, all three versions of MP^{3}C (QP, approximate QP and DB) yield the same performance results shown in Table II for the DB version. They effectively reproduce the OPP performance, thus generating the minimum current

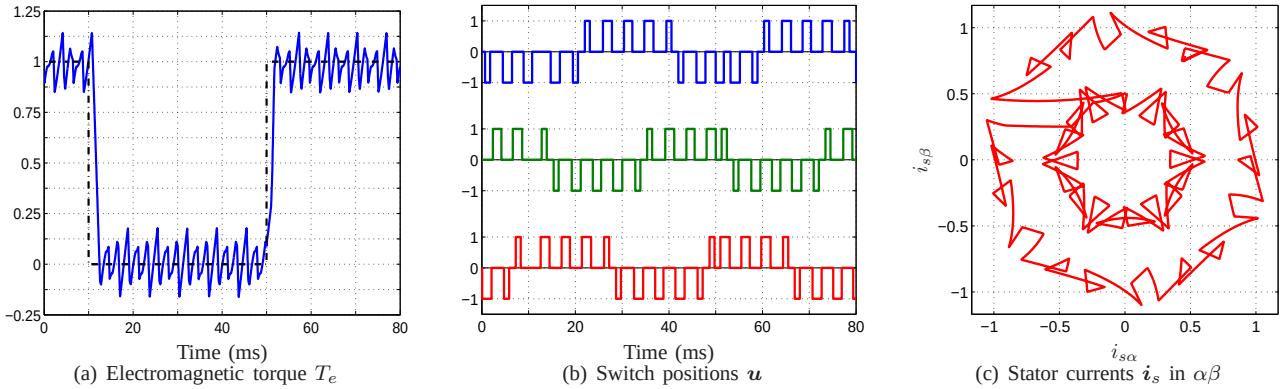

(a) Electromagnetic torque T_e (b) Switch positions $\boldsymbol{u}$ (c) Stator currents $\boldsymbol{i}_s$ in $\alpha\beta$

Fig. 11: Model predictive pulse pattern control (MP^{3}C) at 50% speed with steps in the torque reference. The torque and the switch positions are shown versus the time-axis in ms, while the stator currents are depicted in the stationary orthogonal coordinates. All quantities are given in pu

and torque THDs. This method is conceptually applicable to the whole speed range. However, for higher pulse numbers, the difference between SVM and OPPs becomes smaller and smaller. Thus for low-speed operation, the advantage of OPPs over SVM is minor and the memory required to hold the OPP increases, making SVM the preferred choice. This is clearly shown in Table II in that the MP^{3}C values come closer to the PWM results as the switching frequency increases—although MP^{3}C is still considerably better than both PWM methods over the range displayed. It can also be noted that the THD performances for the two PWM methods is quite similar.

The current waveform and spectrum along with the phase leg switch positions are shown for SVM and MP^{3}C DB modulation respectively in Figs. 9 and 10. These figures refer to the fifth and sixth row in the table, i.e. the middle switching frequency considered in the comparison. From the current waveforms it is readily apparent that MP^{3}C produces a much lower current ripple. Correspondingly, the harmonic components of the MP^{3}C current spectrum are much reduced, particularly regarding the harmonics around f_c and the 17th harmonic.

Notable differences between the QP and the DB version exist in the presence of observer noise. The details will be described in a follow-up paper.

B. Torque Steps

As shown in Fig. 11, at the time-instants of 10 ms and 50 ms steps in the torque reference from 1 pu to 0 pu and back to 1 pu were applied using MP^{3}C with DB control. The settling time is in the range of a few ms and thus similar to those for standard DB and hysteresis control schemes. The MP^{3}C methods based on QP and the approximate solution of the QP (using an active set method), respectively, lead to slower torque response times. Specifically, depending on the weight q and the horizon length, these response times are slower by a factor of two to three.

VII. Conclusions

This paper proposed a new model predictive controller based on optimized pulse patterns that resolves the classic contradiction inherent to drive control—very fast control during transients on the one hand, and optimal performance at steady-state operating conditions on the other, i.e. minimal current THD for a given switching frequency. The former is typically achieved only by deadbeat control schemes and direct torque control, while the latter is in the realm of pre-calculated optimized pulse patterns. The proposed controller, MP^{3}C, achieves both objectives, by adopting the principles of constrained optimal control and receding horizon policy. This method inherently provides robustness, while respecting the optimal volt-second balance of the OPPs under quasi steady-state and dynamic conditions. The result are very fast current and torque responses during transients and very low harmonic distortion levels per switching frequency at steady-state operating conditions.

References

[1] H. S. Patel and R. G. Hoft. Generalized techniques of harmonic elimination and voltage control in thyristor inverters: Part I–Harmonic elimination. *IEEE Trans. Ind. Appl.*, 9(3):310–317, May/Jun. 1973.

[2] G. S. Buja. Optimum output waveforms in PWM inverters. *IEEE Trans. Ind. Appl.*, 16(6):830–836, Nov./Dec. 1980.

[3] J. Holtz and B. Beyer. Fast current trajectory tracking control based on synchronous optimal pulsewidth modulation. *IEEE Trans. Ind. Appl.*, 31(5):1110–1120, Sep./Oct. 1995.

[4] J. Holtz and B. Beyer. The trajectory tracking approach—A new method for minimum distortion PWM in dynamic high-power drives. *IEEE Trans. Ind. Appl.*, 30(4):1048–1057, Jul./Aug. 1994.

[5] B. Beyer. *Schnelle Stromregelung für Hochleistungsantriebe mit Vorgabe der Stromtrajektorie durch off-line optimierte Pulsmuster*. PhD thesis, Wuppertal University, 1998.

[6] J. Holtz and N. Oikonomou. Synchronous optimal pulsewidth modulation and stator flux trajectory control for medium-voltage drives. *IEEE Trans. Ind. Appl.*, 43(2):600–608, Mar./Apr. 2007.

[7] N. Oikonomou and J. Holtz. Stator flux trajectory tracking control for high-performance drives. In *Proc. IEEE Ind. Appl. Soc. Annu. Mtg.*, volume 3, pages 1268–1275, Tampa, FL, USA, Oct. 2006.

[8] N. Oikonomou and J. Holtz. Estimation of the fundamental current in low-switching-frequency high dynamic medium-voltage drives. *IEEE Trans. Ind. Appl.*, 44(5):1597–1605, Sep./Oct. 2008.

[9] C. E. Garcia, D. M. Prett, and M. Morari. Model predictive control: Theory and practice—A survey. *Automatica*, 25(3):335–348, Mar. 1989.

[10] D. Q. Mayne, J. B. Rawlings, C. V. Rao, and P. O. M. Scokaert. Constrained model predictive control: Stability and optimality. *Automatica*, 36(6):789–814, Jun. 2000.

[11] J. B. Rawlings and D. Q. Mayne. *Model predictive control: Theory and design*. Nob Hill Publ., Madison, WI, USA, 2009.

[12] A.K. Rathore, J. Holtz, and T. Boller. Synchronous optimal pulsewidth modulation for low-switching-frequency control of medium-voltage multilevel inverters. *IEEE Trans. Ind. Electron.*, 57(7):2374–2381, Jul. 2010.

[13] J. Nocedal and S. J. Wright. *Numerical Optimization*. Springer, New York, 1999.

[14] B. P. McGrath, D. G. Holmes, and T. Lipo. Optimized space vector switching sequences for multilevel inverters. *IEEE Trans. Power Electron.*, 18(6):1293–1301, Nov. 2003.